Oxidative stress is tightly regulated by cytochrome *c* phosphorylation and respirasome factors in mitochondria

Alejandra Guerra-Castellano[a], Antonio Díaz-Quintana[a], Gonzalo Pérez-Mejías[a], Carlos A. Elena-Real[a], Katiuska González-Arzola[a], Sofía M. García-Mauriño[a], Miguel A. De la Rosa[a,1], and Irene Díaz-Moreno[a,1]

[a]Instituto de Investigaciones Químicas–Centro de Investigaciones Científicas Isla de la Cartuja, Universidad de Sevilla–Consejo Superior de Investigaciones Científicas, 41092 Sevilla, Spain

Edited by Alan R. Fersht, Gonville and Caius College, Cambridge, United Kingdom, and approved June 26, 2018 (received for review April 20, 2018)

Respiratory cytochrome *c* has been found to be phosphorylated at tyrosine 97 in the postischemic brain upon neuroprotective insulin treatment, but how such posttranslational modification affects mitochondrial metabolism is unclear. Here, we report the structural features and functional behavior of a phosphomimetic cytochrome *c* mutant, which was generated by site-specific incorporation at position 97 of *p*-carboxymethyl-L-phenylalanine using the evolved tRNA synthetase method. We found that the point mutation does not alter the overall folding and heme environment of cytochrome *c*, but significantly affects the entire oxidative phosphorylation process. In fact, the electron donation rate of the mutant heme protein to cytochrome *c* oxidase, or complex IV, within respiratory supercomplexes was higher than that of the wild-type species, in agreement with the observed decrease in reactive oxygen species production. Direct contact of cytochrome *c* with the respiratory supercomplex factor HIGD1A (hypoxia-inducible domain family member 1A) is reported here, with the mutant heme protein exhibiting a lower affinity than the wild-type species. Interestingly, phosphomimetic cytochrome *c* also exhibited a lower caspase-3 activation activity. Altogether, these findings yield a better understanding of the molecular basis for mitochondrial metabolism in acute diseases, such as brain ischemia, and thus could allow the use of phosphomimetic cytochrome *c* as a neuroprotector with therapeutic applications.

cytochrome *c* | electron transport chain | oxidative stress | phosphorylation | reactive oxygen species

Cell redox signaling is fine-tuned by protein phosphorylation, a well-known posttranslational modification in turn modulated by the antagonistic effects of kinases and phosphatases (1, 2). Such an interplay is specifically relevant in mitochondrial metabolism, which is the main source of reactive oxygen species/reactive nitrogen species (ROS/RNS) in the cell (3). Tyrosine kinases, in particular, are key signaling mediators and their perturbations underlie many human pathologies, namely cancer and neurodegenerative diseases (4, 5). One of the main proteins that control redox signaling in mitochondrial oxidative phosphorylation (OxPhos) is cytochrome *c* (C*c*), the functions of which are regulated by phosphorylation of several residues (6–10).

C*c* plays a double role in the cellular metabolism. Under homeostasis, C*c* is located in the mitochondrial intermembrane space, where it acts as an electron carrier between complex III (CIII) and complex IV (CIV) in the electron transfer chain (ETC). These two respiratory complexes can be either independent or associated with each other and with complex I (CI), thus forming mitochondrial supercomplexes—the so-called respirasome—the assembly of which is strictly dependent on metabolic needs (11). Respiratory supercomplexes provide higher efficiency to the electron transport during OxPhos, thereby minimizing the generation of ROS (12). Respiratory supercomplex factors (Rcfs) are protein modulators that stabilize the membrane-embedded CIII and CIV within respiratory supercomplexes. These factors have been found in both yeasts and mammals. In yeasts, they are called respiratory supercomplex factor 1 (Rcf1, formerly Aim31) and respiratory supercomplex factor 2 (Rcf2, formerly Aim38), both being members of the conserved hypoxia-induced gene 1 (Hig1) protein family (13, 14). Rcf1 has two human orthologs, namely the HIG hypoxia-inducible domain family members 1A and 2A (HIGD1A and HIGD2A, respectively) (15). Rcf2, in contrast, is yeast-specific and necessary for oligomerization of a subclass of C*c* oxidase (C*c*O) into supercomplexes.

Under nitro-oxidative stress conditions, C*c* acts as a programmed cell death (PCD) inducer (16). During early apoptosis, a C*c* population—tightly bound to the mitochondrial membrane—triggers peroxidation of phospholipids and, in particular, of cardiolipin (CL). CL-adducted C*c* undergoes a profound tertiary conformational rearrangement that opens an entry channel for H_2O_2 molecules, which explains how C*c* enhances its peroxidase activity (17, 18). It has been proposed that C*c*-CL conjugates are sufficient for formation of mitochondrial pores, allowing the release of the hemeprotein into the cytosol during apoptosis (19).

Extramitochondrial C*c* binds to the apoptotic protease-activating factor 1 (Apaf1), thereby eliciting the apoptosome

Significance

Dysfunction of mitochondria, the powerhouses of living cells, favors the onset of human diseases, namely neurodegenerative diseases, cardiovascular pathologies, and cancer. Actually, respiratory cytochrome *c* has been found to be phosphorylated at tyrosine 97 during the insulin-induced neuroprotection response following a brain ischemic injury. Here, we report that the decrease in neuronal death could be directly ascribed to changes in mitochondrial metabolism—including lower production of reactive oxygen species—and cell homeostasis induced by cytochrome *c* phosphorylation. Our findings thus provide the basis for understanding the molecular mechanism and potential use of phosphomimetic species of cytochrome *c*, thereby yielding new opportunities to develop more efficient therapies against acute pathologies.

Author contributions: A.G.-C., A.D.-Q., M.A.R., and I.D.-M. designed research; A.G.-C., G.P.-M., C.A.E.-R., K.G.-A., S.M.G.-M., and I.D.-M. performed research; A.G.-C., A.D.-Q., G.P.-M., C.A.E.-R., and I.D.-M. analyzed data; and A.G.-C., A.D.-Q., M.A.R., and I.D.-M. wrote the paper.

The authors declare no conflict of interest.

This article is a PNAS Direct Submission.

[1]To whom correspondence may be addressed. Email: marosa@us.es or idiazmoreno@us.es.

This article contains supporting information online at www.pnas.org/lookup/suppl/doi:10.1073/pnas.1806833115/-/DCSupplemental.

Published online July 17, 2018.

Table 1. Midpoint melting temperature (T_m) (°C) of WT and Y97*p*CMF C*c*

Cc species	Far-UV CD, 220 nm	Visible CD, 419 nm	Fluorescence, 270 nm
WT	88.6 ± 1.9	43.9 ± 2.0 (T_{m1}) 85.1 ± 2.3 (T_{m2})	86.3 ± 1.4
Y97*p*CMF	82.2 ± 0.3	76.6 ± 4.9	82.6 ± 1.6

platform assembly and activating the caspase cascade (20, 21). Recent data indicate that the programmed cell death network involving C*c* is complex, and that C*c* targets several proteins that are functionally equivalent in humans and plants (22–24). In both type of cells, for example, C*c* reaches the cell nucleus upon DNA damage and sequesters human SET/TAF1β and plant NRP1 histone chaperones that remodel chromatin (25–27).

In addition to regulating the functions described above, phosphorylated C*c* species have been associated with several human pathologies. In fact, it has been proposed that Tyr97 is target of phosphorylation during the insulin-induced neuroprotection response following a brain ischemic injury (28). A possible mechanism could be that Tyr97 phosphorylation of C*c* would alter the electron shuttling to C*c*O (7). Notably, electron transfer from wild-type (WT) C*c* to C*c*O is positively regulated by the HIGD1A membrane protein (29).

Research on tyrosine phosphorylation of C*c* has normally resorted to using Tyr-to-Glu mutations (30, 31). This overcomes the difficulties of obtaining enough phosphorylated C*c* for biophysical and functional studies when the specific C*c*-phosphorylating kinase is unknown (32). However, the Tyr-to-Glu substitution leads to a substantial decrease in the residue volume and the loss of an aromatic ring. Therefore, we used the evolved tRNA synthetase technique to introduce the noncanonical amino acid *p*-carboxymethyl-L-phenylalanine (*p*CMF) at position 97, as previously reported for Tyr48 (33). This noncanonical amino acid is actually used to synthesize stable analogs of a wide array of phosphoproteins, the kinases of which are unknown or the yields of which from tissues are low. In addition, *p*CMF provides a dependable analog of phosphorylated tyrosine that can be used to study signal transduction pathways. In this work, the resulting Y97*p*CMF C*c* mutant maintained its overall folding and heme environment. We found that such a post-translational modification of C*c* affected the OxPhos process since it enhanced the electron donation rate to C*c*O in mitochondria isolated from yeasts grown in respiratory metabolism. In addition, we observed a decrease in the production of ROS. Thus, the C*c*O-driven oxidation rate of C*c* is controlled by

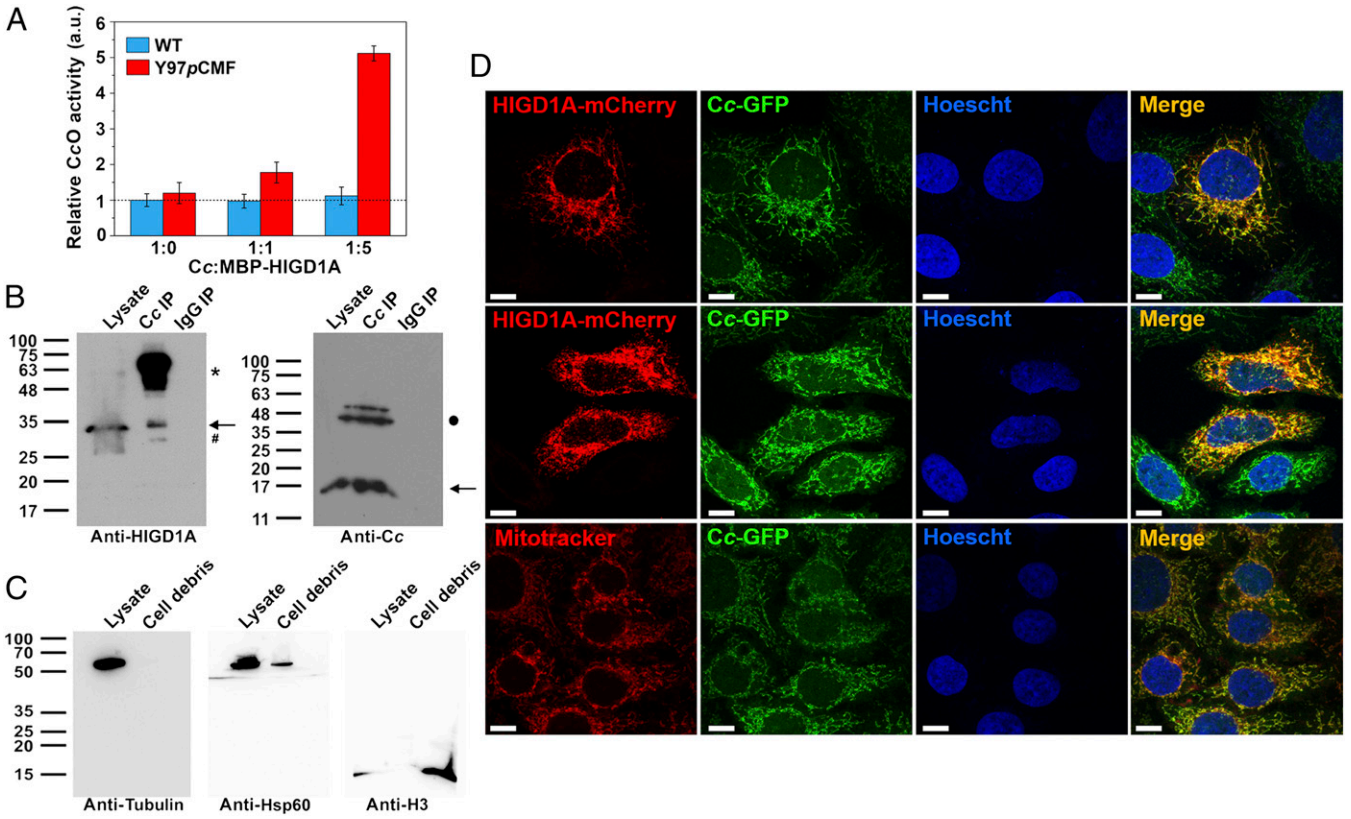

Fig. 1. Modulation of C*c*O activity by the HIGD1A protein and interaction of the latter with C*c*. (*A*) Bovine C*c*O activity with added WT (blue) or Y97*p*CMF (red) C*c* as electron donor in the presence of the chimera MBP-HIGD1A at varying concentrations. The 1:0 bars represent the C*c*O activity without MBP-HIGD1A. Experimental data were normalized to the C*c*:HIGD1A ratio of 1:0 for WT C*c* species. a.u.: arbitrary units. (*B*) Immunoprecipitation of transfected HIGD1A-mCherry with C*c* in Heltog cells. (*Left*) Western blot shows the detection of the HIGD1A-mCherry band in the lysates, along with C*c*-IP of lysates followed by probing with the HIGD1A antibody (arrow). Mouse IgG (IgG) was used as control. (*Right*) Detection of C*c* band in lysates and C*c*-immunoprecipitated lysates are also shown (arrow). Asterisks and hashtags are heavy and light chains of IgG, respectively. The black circle stands for unspecific bands of anti-C*c* antibody, as reported by the manufacturer. (*C*) Western blots against cytosolic (tubulin), mitochondrial (Hsp60), and nuclear (H3) markers. (*D*) Subcellular localization of HIGD1A and C*c* proteins by confocal microscopy. Heltog cells were transfected to express the chimera HIGD1A-mCherry (red; first column of *Upper* and *Middle* rows). The chimera C*c*-GFP is stably expressed in the Heltog cell line (green; second columns). Nuclei were stained in blue with Hoechst (third columns) and mitochondria with MitoTracker Red CMXRos (red, first panel of *Lower* row). Colocalization between green C*c*-GFP and red HIGD1A-mCherry in mitochondria, along with blue nuclear staining, is shown in the merge images (last columns of *Upper* and *Middle* rows). (Scale bars: 10 μm.)

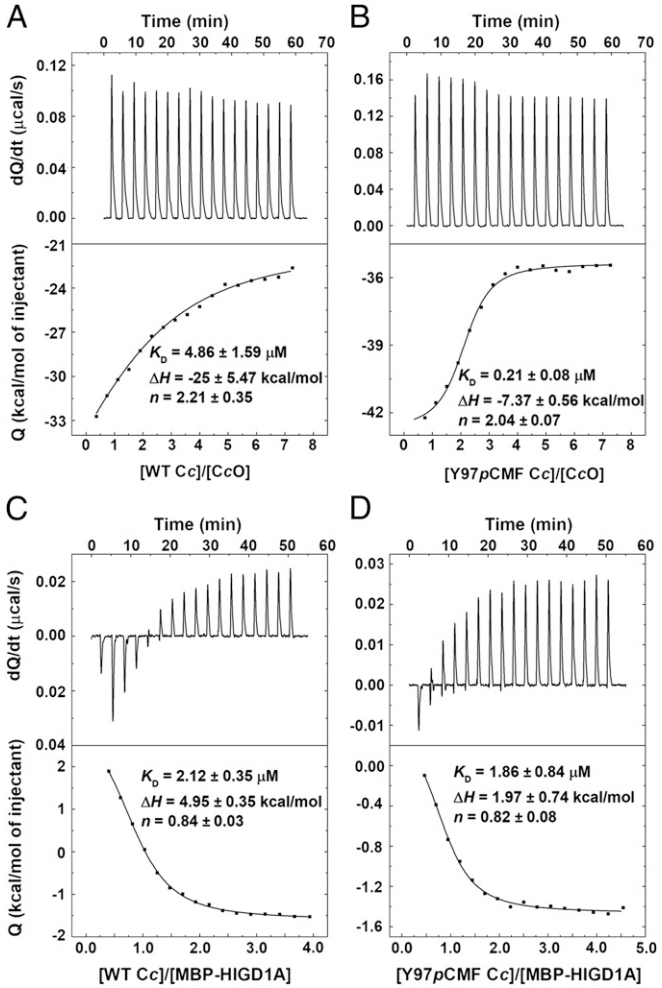

Fig. 2. ITC assays of CcO and HIGD1A with WT and Y97*p*CMF Cc. (*A* and *B*) Thermograms (*Upper*) and binding isotherms (*Lower*) of WT Cc/CcO (*A*) and Y97*p*CMF Cc/CcO (*B*) complexes in their reduced states. Experimental data were fitted to a 2:1 model with the same K_D values. (*C* and *D*) Thermograms (*Upper*) and binding isotherms (*Lower*) of WT Cc/MBP-HIGD1A (*C*) and Y97*p*CMF Cc/MBP-HIGD1A (*D*) complexes at reduced states. Data were fitted to a model with a 1:1 stoichiometry.

phosphorylation to maintain low levels of apoptotic-inducing ROS. Furthermore, Y97*p*CMF Cc was an inefficient caspase activator. Altogether, these findings can shed light on the function of phosphorylated Cc in insulin-stimulated postischemic neuroprotection.

Results and Discussion

Substitution of Tyr97 with *p*CMF Allows for Study of Cc Phosphorylation, Preserving Its Physicochemical Properties. To accurately study the phosphorylation of Cc at Tyr97, this residue was substituted with the noncanonical amino acid *p*CMF, which is an analog of phosphotyrosine residue. To do that, we used the evolved tRNA synthetase method as previously reported (*SI Appendix*, Fig. S1). As described above, this substitution simulates the charge and the volume of a phosphotyrosine residue better than a glutamate substitution (33).

To confirm that the noncanonical amino acid *p*CMF was successfully introduced at position 97 of the heme protein, the Y97*p*CMF Cc mutant was purified to homogeneity, and its molecular mass was compared with that of WT Cc by MALDI-TOF (*SI Appendix*, Fig. S2 *A* and *B*). The phosphomimetic mutant presented an increase of 41 Da in its molecular mass in comparison with that of WT Cc, which is consistent with the expected substitution (*SI Appendix*, Fig. S2*A*). To check whether the amino acid replacement affected the secondary structure and heme environment of Cc, circular dichroism (CD) spectroscopy measurements in the far-UV and visible region were carried out, respectively. Those data demonstrated that Y97*p*CMF Cc exhibited an overall secondary structure and heme properties similar to those observed for WT Cc (*SI Appendix*, Fig. S2 *C* and *D*).

Following with the biophysical analysis of the Y97*p*CMF mutant, the alkaline transition phenomenon was also analyzed. This phenomenon has been related to a change in the Cc cell location, which is essential for its role in PCD (34). Such transition affects the oxidized form of Cc and involves the replacement of Met80—the sixth ligand of the heme group—by Lys72, Lys73, or Lys79 as an axial ligand at high pH values (35). To analyze the Fe-Met80(S_δ) bond changes induced by pH, we therefore monitored the charge-transfer band at 699 nm, which disappears concomitantly with the alkaline transition (*SI Appendix*, Fig. S3*A*) (36). The quantitative analysis yields a difference of ∼0.8 in the pK_a values for this alkaline transition in the WT and Y97*p*CMF Cc species (p$K_{a\text{-WT}}$ = 8.9 ± 0.4 and p$K_{a\text{-Y97}p\text{CMF}}$ = 8.1 ± 0.2; *SI Appendix*, Fig. S3 *B–D*).

On the other hand, given that most mutations in Tyr97 performed to date alter the thermal stability of Cc, we explored that possibility in Y97*p*CMF Cc (31, 37). In terms of secondary and overall structure, data from far-UV CD and fluorescence, respectively, showed that the midpoint melting temperature (T_m) of Y97*p*CMF was slightly lower than that calculated for WT Cc (Table 1). Notably, in contrast to the data recorded for the heme group environment of WT species, the visible CD data of Y97*p*CMF Cc fit well into a two-state model (Table 1). Such findings could indicate a slight destabilization in the N-terminal α-helix pack, which constitutes an early event in Cc folding (38–41).

Altogether, the biophysical comparison of WT and Y97*p*CMF Cc species indicates that the substitution of Tyr97 with noncanonical *p*CMF is a good approach to studying the consequences of Cc phosphorylation without significantly altering the physicochemical and structural properties.

CcO Activity Is Modulated by Y97*p*CMF Cc and Respiratory Supercomplex Factors. Given that phosphorylation of Cc has been described as a phenomenon that modulates the functions of this metalloprotein, we explored the behavior of Y97*p*CMF Cc as an electron donor. The in vitro ability of Y97*p*CMF Cc to reduce CcO was measured in the absence or presence of HIGD1A, which acts as a positive modulator of CcO (29). In the absence of a modulator, the CcO activities were slightly higher with the Y97*p*CMF mutant compared with the WT Cc (Fig. 1*A*). Then we wondered whether those slight changes were due to a change in the molecular recognition mode between both Cc species and CcO. Thus, we analyzed the interaction between CcO and WT or phosphomimetic Y97*p*CMF Cc by isothermal titration calorimetry (ITC) (Fig. 2*A* and *B*). Both isotherms were fitted to a model with two independent binding sites, as previously described for the cross-complex between human WT Cc and bovine CcO (42). Notably, the K_D values showed that Y97*p*CMF Cc had a higher affinity for CcO than did the WT species. These results would explain the higher CcO activity shown by the phosphomimetic mutant.

Recently, it has been described that the HIGD1A-dependent increase in CcO activity was higher with a Cc phosphomimetic mutant at position 48 (9). For this reason, we tested the effect of the HIGD1A in CcO activity through WT and Y97*p*CMF Cc. To avoid the solubility problem of the membrane protein HIGD1A, we used a chimera with a maltose binding protein (MBP) tag in its N terminus (MBP-HIGD1A) (*SI Appendix*, Fig. S4). Notably, CcO activity significantly increased upon addition of MBP-HIGD1A through Y97*p*CMF Cc (Fig. 1*A*). To discard a possible contribution from

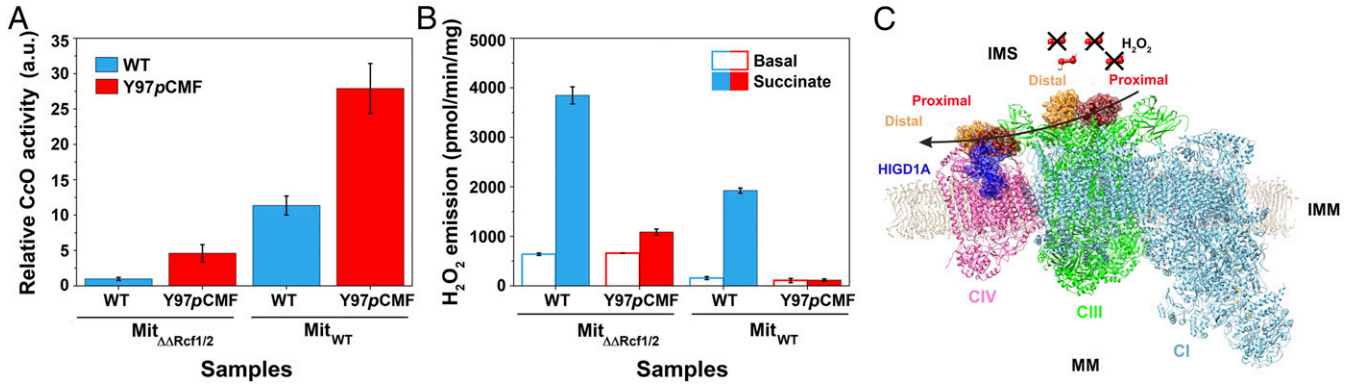

Fig. 3. Effect of the respiratory factors on CcO activity and ROS production in isolated mitochondria. (*A*) CcO activity was measured in isolated mitochondria with added WT Cc (blue bars) or Y97*p*CMF Cc (red bars). Data were normalized with respect to the activity with WT Cc in mitochondria isolated from ΔΔRcf1/2 yeast strains. Data represent the mean ± SD of three independent experiments. a.u.: arbitrary units. (*B*) H_2O_2 production in isolated $Mit_{\Delta\Delta Rcf1/2}$ and Mit_{WT}. ROS generation was triggered by addition of succinate. Bar color code is the same as in *A*. (*C*) Molecular model of OxPhos and ROS production by respirasome when Cc is phosphorylated. The CcO-driven oxidation rate of Cc is facilitated by Tyr-97 phosphorylation and supercomplex formation to maintain low levels of apoptotic-inducing ROS. Blue, CI; green, dimeric CIII; and magenta, CIV. Cc molecules at the proximal sites of one monomer of CIII or CIV are in red, whereas those at the distal sites are in yellow. HIGD1A, colored in dark blue, makes contacts with CIV and the molecule of Cc located at its proximal site. The black arrow indicates the channeling of Cc molecules between CIII and CIV. IMM, inner mitochondrial membrane; IMS, intermembrane mitochondrial space; MM, mitochondrial matrix.

the MBP tag in C*c*O activity, assays were also performed with MBP protein in the presence of both C*c* species. As shown in *SI Appendix*, Fig. S5*A*, MBP did not alter C*c*O activity.

Taking into account the differences observed in Fig. 1*A*, we would expect an eventual interaction between C*c* and HIGD1A. To explore this further, we examined the interaction between MBP-HIGD1A and WT or Y97*p*CMF C*c* by ITC (Fig. 2 *C* and *D*). These measurements revealed that both C*c* species interacted with MBP-HIGD1A with a stoichiometry of 1:1, yielding dissociation constant (K_D) values within the micromolar range. To demonstrate that the interaction with the chimera was uniquely due to the HIGD1A module, we performed an ITC assay between WT C*c* and the MBP protein (*SI Appendix*, Fig. S5*B*). These data revealed the absence of any interaction between both proteins. In addition, dilution ITC experiments showed that the observed changes in heat rate are rather due to the interaction between the C*c* species and MBP-HIGD1A (*SI Appendix*, Fig. S6 *A* and *B*). The redox state of C*c* did not affect its interaction with HIGD1A (*SI Appendix*, Fig. S6*C*). Since the N-terminal domain of HIGD1A—hereafter, $HIGD1A_{1–26}$—has been reported to retain C*c* in the intermembrane mitochondrial space (IMS) and to decrease caspase activation (43), a set of ITC titrations were run. Data resulting from such titrations evinced that both C*c* species interacted with $HIGD1A_{1–26}$ with similar stoichiometry values, although Y97*p*CMF C*c* showed less affinity than WT C*c* (*SI Appendix*, Fig. S7). Thus, the lesser affinity of Y97*p*CMF C*c* toward $HIGD1A_{1–26}$ or MBP-HIGD1A may point out a higher interaction turnover of the phosphomimetic mutant in comparison with the WT species, thus facilitating C*c*O reduction (Fig. 1*A*).

To test the interaction between HIGD1A and C*c* in cells, coimmunoprecipitation (Co-IP) assays were performed in Heltog cells—HeLa cells constitutively expressing green fluorescent protein (GFP)-tagged C*c*—transfected with HIGD1A-mCherry vector. Immunoblotting data against HIGD1A corroborated the interaction between C*c* and HIGD1A (Fig. 1*B*). The total lysate used in the Co-IP assays contained cytosolic and mitochondrial fractions, as shown by the detection of tubulin and Hsp60, respectively (Fig. 1*C*). Furthermore, we checked that both C*c* and HIGD1A were in the same cellular compartment by confocal analysis of Heltog cells upon transfection with HIGD1A-mCherry vector, which codes for red fluorescence-tagged proteins. The pictures showed that C*c*-GFP (green fluorescence) colocalized with HIGD1A-mCherry (red fluorescence) under homeostatic conditions (Fig. 1*D*, *Upper* and *Middle*). The mitochondrial localization of C*c*-GFP was confirmed by codetection with the MitoTracker (Fig. 1*D*, *Lower*). Altogether, these findings revealed contacts between HIGD1A and C*c* species.

Based on these results, the HIGD1A- and C*c* phosphorylation-mediated regulations of C*c*O activity were tested in a cellular context using isolated mitochondria from yeast cells grown on a respiratory media. Under such growth conditions, Rcf1—a yeast ortholog of human HIGD1A—and Rcf2 stabilized the CIII–CIV interaction, favoring the formation of the supercomplexes (13, 14, 44). To analyze the effect of supercomplex formation, we used mitochondria obtained from WT and Rcf1/Rcf2-deficient yeast strains (Mit_{wt} and $Mit_{\Delta\Delta Rcf1/2}$, respectively). The supercomplex formation was impaired in $Mit_{\Delta\Delta Rcf1/2}$ due to the absence of Rcf1 and Rcf2 proteins (*SI Appendix*, Figs. S5*C* and S8). In fact, C*c*O activity assays using $Mit_{\Delta\Delta Rcf1/2}$ revealed an electron flow significantly lower in comparison with those observed using Mit_{WT}, regardless whether WT or Y97*p*CMF C*c* was added (Fig. 3*A*). In addition, a single deletion of either Rcf1 or Rcf2 partially affected the C*c*O activity levels, indicating a cooperative effect when the two membrane proteins Rcf1 and Rcf2 were present (*SI Appendix*, Fig. S5*C*). Notably, the Y97*p*CMF C*c* mutant exhibited higher C*c*O activity than WT C*c*, both in WT (Mit_{WT}) and in mutant mitochondria ($Mit_{\Delta Rcf1}$, $Mit_{\Delta Rcf2}$, and $Mit_{\Delta\Delta RCf1/2}$) (Fig. 3*A* and *SI Appendix*, Fig. S5*C*). This finding indicates that the Rcf-mediated ETC flow is more efficient when Y97*p*CMF C*c* participates (Fig. 3*A*). This suggests a double regulation mechanism through C*c* phosphorylation and supercomplex formation to make an accurate cellular response against hypoxia or other respiratory stresses and needs.

Y97*p*CMF C*c* Impairs Mitochondrial Supercomplex-Mediated ROS Production. Changes in the ETC flow can affect the hyperpolarization of mitochondrial inner membrane and ROS production (45). For this reason, we investigated if the accelerated C*c*O-driven oxidation rate of phosphorylated C*c* could alter mitochondrial ROS production both in the absence and in the presence of respiratory supercomplexes. ROS production in mitochondria from *Saccharomyces cerevisiae* occurs mainly in CIII as its mitochondria are deficient in CI (46, 47). Significant contribution of complex II (CII) to ROS generation has recently been described in mammalian mitochondria (48–50). In *S. cerevisiae*, however, contribution of CII to ROS generation occurs only when specific mutations are present near the proximal quinone-binding

site (Q_P) of CII (51). Since our study was focused on C*c*-mediated ROS production, with C*c* acting as an electron donor between CIII and CIV, no ETC inhibitors were used. Therefore, succinate was added as electron donor to both types of mitochondria, in the presence of either WT or Y97*p*CMF C*c*, to trigger the ETC through CII. Upon addition of succinate, ETC-dependent H_2O_2 production significantly increased, especially in $Mit_{\Delta\Delta Rcf1/2}$ where the formation of supercomplexes is impaired (Fig. 3*B* and *SI Appendix*, Fig. S9). Remarkably, Y97*p*CMF C*c* made ROS production decrease in $Mit_{\Delta\Delta Rcf1/2}$ and, more pronouncedly, in Mit_{WT} where supercomplexes are formed (Fig. 3*B*). These findings suggest that the C*c*O-driven oxidation rate of C*c* is tightly regulated by C*c* phosphorylation and supercomplex formation to keep apoptotic-inducing mitochondrial ROS at a low level.

Thus, we propose a respirasome OxPhos model based on the recently described extra distal C*c*-binding sites in CIII and CIV, thus providing a path for diffusion of C*c* molecules (Fig. 3*C*) (42, 52). This way of communicating between complexes through Tyr97-phosphorylated C*c* could accelerate the electron transfer flow, which, in turn, would avoid ROS-mediated cellular damage to guarantee neuronal survival during ischemia reperfusion in the brain (28, 45).

ROS Scavenger Activity and Cardiolipin Binding of C*c* Remains Unaltered upon Phosphorylation. We wondered whether the low levels of ROS displayed by the presence of Y97*p*CMF C*c* might be caused by an exacerbated peroxidase activity of the heme protein. We thus measured such enzymatic activity in WT and mutant C*c*, either free or bound to lipid vesicles containing CL at a 4:1 ratio [1,2-dioleoyl-*sn*-glycero-3-phosphocholine:1,1′2,2′-tetraoleoylcardiolipin (DOPC:TOCL)]. No differences in peroxidase activity were observed between Y97*p*CMF and WT C*c* species, both when free or bound to liposomes. It should be noted that the use of liposomes rose the peroxidase activity considerably, although in the same way for WT and phosphomimetic C*c* (Fig. 4*A*). This finding corroborates that the drop in ROS production upon mitochondrial supercomplex assembly is due to a more efficient C*c*O-driven oxidation rate by Y97*p*CMF than by WT C*c*.

In addition, the onset of PCD is triggered by the ability of the hemeprotein to leave the mitochondria after binding to CL (53). Therefore, a plausible hypothesis is that the decrease in neuronal ischemic death may be due to a less efficient release of phosphorylated C*c* to the cytosol, concomitantly with its role as a PCD inducer. Hence, we examined the binding of C*c* species to liposomes containing CL (DOPC:TOCL) (4:1) or not (DOPC) by electrophoretic mobility shift assays (EMSA) in native agarose gels (*SI Appendix*, Fig. S10). The electrophoretic mobility of Y97*p*CMF and WT C*c* species shifted in the same manner upon DOPC:TOCL liposome additions, unveiling that both C*c* species were able to bind to CL (*SI Appendix*, Fig. S10). Likewise, EMSA data showed that none of the C*c* species had altered the electrophoretic mobility with DOPC liposomes, corroborating that the two C*c* species specifically interact with CL and not with other lipids of the inner mitochondrial membrane. To sum up, these data showed that there is no evidence that phosphorylated C*c* at Tyr97 is preferably retained in the mitochondria.

Y97*p*CMF C*c* Is an Inefficient Caspase Activator. In the context of ischemic brain damage, inhibition of both C*c*–Apaf1 interaction and caspase-3 cleavage constitutes a potent neuroprotective strategy (54, 55). The binding assays involving C*c*, HIGD1A, and CL suggested that both WT and Y97*p*CMF C*c* species did seem to be equally retained in mitochondria. Therefore, the neuroprotective role of phosphorylated C*c* cannot be fully explained by a specific sequestration of Y97*p*CMF C*c* in the IMS. Thus, we explored whether phosphorylation at Tyr97 modulated C*c* ability to trigger the caspase cascade in the cytosol, where the hemeprotein interacts with Apaf1 to assemble the so-called apoptosome.

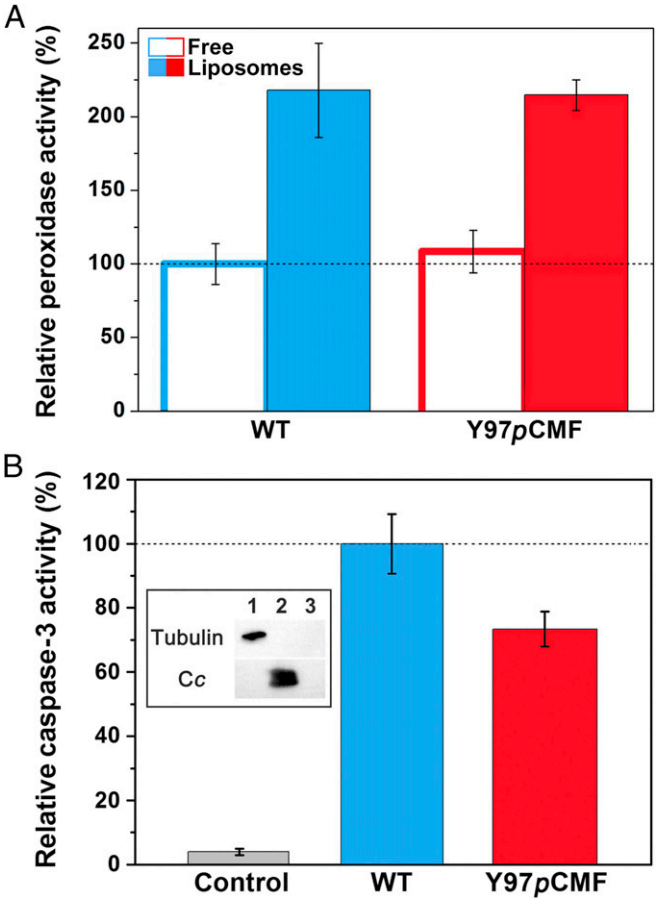

Fig. 4. Peroxidase and caspase activities of Y97*p*CMF Cc. (*A*) Peroxidase activity of WT C*c* (blue) and Y97*p*CMF C*c* (red) either free (empty bars) or in the presence of liposomes containing DOPC:TOCL (4:1) (filled bars). Data represent the mean ± SD of three independent experiments and are normalized to the peroxidase activity of free WT C*c*. (*B*) Caspase-3 activity upon addition of exogenous WT (blue) or Y97*p*CMF (red) C*c*. Caspase auto-activation, in the absence of added C*c*, was also tested (control bar). Data represent the mean ± SD of three independent experiments and are normalized with respect to the activity determined with WT C*c*. (*Inset*) Western blots confirmed the lack of endogenous C*c* in the cytoplasmic cell extracts by immunoblotting with anti-tubulin (cytosolic marker) and anti-C*c* antibodies. Lane 1, cytoplasmic cell extracts; lane 2, purified C*c*; and lane 3, BSA as a negative control.

We analyzed the caspase-3 activation driven by WT and Y97*p*CMF C*c*, using cytoplasmic extracts of human embryonic kidney 293 cells that lack C*c* (Fig. 4*B*). The Y97*p*CMF C*c*-mediated caspase-3 activity decreased by about 26% with respect to that mediated by WT C*c* (Fig. 4*B*). These findings agree with our previous results on Y97E and Y97F C*c* mutants, as well as with the nitrated mono-Tyr97 C*c*, which have a caspase activation slightly lower than that of the WT species (31, 56). Interestingly, none of these C*c* species disrupted the C*c*/Apaf1 complex assembly, and this is also expected for the Y97*p*CMF form. However, the formation of a nonfunctional apoptosome upon posttranslational modifications of C*c* cannot be excluded (31, 56, 57).

Altogether, our data suggest that both low oxidative stress in mitochondria and less activation of the caspase cascade in cytoplasm explain neuronal survival under ischemia damage in cells containing Tyr97-phosphorylated C*c*.

Materials and Methods

Expression of genes in *Escherichia coli* and purification of C*c* and HIGD1A protein constructs followed standard procedures. All experimental conditions are further available in *SI Appendix*, including strains, culture

conditions, cell transfection experiments, cell-extract fraction analyses, thermal analyses, and enzymatic activity assays. All biological samples were obtained from bacteria, yeast, or human cell extracts in full compliance with University of Seville Ethical Committee bylaws.

ACKNOWLEDGMENTS. We thank Prof. P. G. Schultz (Scripps Research Institute) for providing the plasmid pEVOL/pCMF/tRNA; Prof. Peter Rehling (University Medical Center Göttingen) for the antibodies αRcf1 and αRcf2; and Dr. Rosemary A. Stuart (Klingler College of Arts and Sciences, Marquette University) for the *S. cerevisiae* strains WT (*W303-1A mata leu2 trp1 ura3 his3 ade2*), RCF1::HIS3 (Δrcf1) (*W303-1A mata leu2 trp1 ura3 ade2*), RCF2::KAN (*Δrcf2*) (*W303-1B Matα leu2 trp1 ura3 his3 ade2*), and RCF1::HIS3 RCF2::KAN (*Δrcf1 Δrcf2*) (*W303-1A mata leu2 trp1 ura3 ade2*). This work was supported by Ministry of Economy and Competitiveness and European Regional Development Fund (MINECO/FEDER) Grant BFU2015-71017/BMC, European Union; the Ramón Areces Foundation, European Social Fund, Andalusian Government (BIO-198); Consejo Superior de Investigaciones Científicas Fellowship JaePre_2011_01248 (to A.G.-C.); a Fundación Cámara PhD Fellowship (to C.A.E.-R.); Biointeractomics Platform (cicCartuja, Seville); and TA Instruments. The INSTRUCT platform of Baculovirus expression (expression screening@OPPF) was used for cloning the HIGD1A into the pOPINM vector.

1. Monteiro HP, Stern A (1996) Redox modulation of tyrosine phosphorylation-dependent signal transduction pathways. *Free Radic Biol Med* 21:323–333.
2. Corcoran A, Cotter TG (2013) Redox regulation of protein kinases. *FEBS J* 280: 1944–1965.
3. Turrens JF (2003) Mitochondrial formation of reactive oxygen species. *J Physiol* 552: 335–344.
4. Sefton BM, Hunter T, Beemon K, Eckhart W (1980) Evidence that the phosphorylation of tyrosine is essential for cellular transformation by Rous sarcoma virus. *Cell* 20:807–816.
5. Ingley E (2012) Functions of the Lyn tyrosine kinase in health and disease. *Cell Commun Signal* 10:21.
6. Hüttemann M, Lee I, Grossman LI, Doan JW, Sanderson TH (2012) Phosphorylation of mammalian cytochrome *c* and cytochrome *c* oxidase in the regulation of cell destiny: Respiration, apoptosis, and human disease. *Adv Exp Med Biol* 748:237–264.
7. Lee I, et al. (2006) New prospects for an old enzyme: Mammalian cytochrome *c* is tyrosine-phosphorylated *in vivo*. *Biochemistry* 45:9121–9128.
8. Yu H, Lee I, Salomon AR, Yu K, Hüttemann M (2008) Mammalian liver cytochrome c is tyrosine-48 phosphorylated in vivo, inhibiting mitochondrial respiration. *Biochim Biophys Acta* 1777:1066–1071.
9. Moreno-Beltrán B, et al. (2017) Structural basis of mitochondrial dysfunction in response to cytochrome *c* phosphorylation at tyrosine 48. *Proc Natl Acad Sci USA* 114: E3041–E3050.
10. Guerra-Castellano A, Díaz-Moreno I, Velázquez-Campoy A, De la Rosa MA, Díaz-Quintana A (2016) Structural and functional characterization of phosphomimetic mutants of cytochrome c at threonine 28 and serine 47. *Biochim Biophys Acta* 1857: 387–395.
11. Ramírez-Aguilar SJ, et al. (2011) The composition of plant mitochondrial supercomplexes changes with oxygen availability. *J Biol Chem* 286:43045–43053.
12. Genova ML, Lenaz G (2014) Functional role of mitochondrial respiratory supercomplexes. *Biochim Biophys Acta* 1837:427–443.
13. Strogolova V, Furness A, Robb-McGrath M, Garlich J, Stuart RA (2012) Rcf1 and Rcf2, members of the hypoxia-induced gene 1 protein family, are critical components of the mitochondrial cytochrome bc_1-cytochrome *c* oxidase supercomplex. *Mol Cell Biol* 32:1363–1373.
14. Vukotic M, et al. (2012) Rcf1 mediates cytochrome oxidase assembly and respirasome formation, revealing heterogeneity of the enzyme complex. *Cell Metab* 15:336–347.
15. Shoubridge EA (2012) Supersizing the mitochondrial respiratory chain. *Cell Metab* 15: 271–272.
16. Ow YP, Green DR, Hao Z, Mak TW (2008) Cytochrome *c*: Functions beyond respiration. *Nat Rev Mol Cell Biol* 9:532–542.
17. Mohammadyani D, et al. (2018) Structural characterization of cardiolipin-driven activation of cytochrome c into a peroxidase and membrane perturbation. *Biochim Biophys Acta* 1860:1057–1068.
18. Vladimirov YA, et al. (2006) Cardiolipin activates cytochrome *c* peroxidase activity since it facilitates $H(_2)O(_2)$ access to heme. *Biochemistry (Mosc)* 71:998–1005.
19. Bergstrom CL, Beales PA, Lv Y, Vanderlick TK, Groves JT (2013) Cytochrome *c* causes pore formation in cardiolipin-containing membranes. *Proc Natl Acad Sci USA* 110: 6269–6274.
20. Zou H, Li Y, Liu X, Wang X (1999) An APAF-1.cytochrome c multimeric complex is a functional apoptosome that activates procaspase-9. *J Biol Chem* 274:11549–11556.
21. Desagher S, Martinou JC (2000) Mitochondria as the central control point of apoptosis. *Trends Cell Biol* 10:369–377.
22. Martínez-Fábregas J, et al. (2013) New *Arabidopsis thaliana* cytochrome *c* partners: A look into the elusive role of cytochrome *c* in programmed cell death in plants. *Mol Cell Proteomics* 12:3666–3676.
23. Martínez-Fábregas J, et al. (2014) Structural and functional analysis of novel human cytochrome *C* targets in apoptosis. *Mol Cell Proteomics* 13:1439–1456.
24. Martínez-Fábregas J, Díaz-Moreno I, González-Arzola K, Díaz-Quintana A, De la Rosa MA (2014) A common signalosome for programmed cell death in humans and plants. *Cell Death Dis* 5:e1314.
25. González-Arzola K, et al. (2015) Structural basis for inhibition of the histone chaperone activity of SET/TAF-Iβ by cytochrome *c*. *Proc Natl Acad Sci USA* 112:9908–9913.
26. González-Arzola K, et al. (2017) Histone chaperone activity of *Arabidopsis thaliana* NRP1 is blocked by cytochrome *c*. *Nucleic Acids Res* 45:2150–2165.
27. Díaz-Moreno I, Velázquez-Cruz A, Curran-French S, Díaz-Quintana A, De la Rosa MA (2018) Nuclear cytochrome *c*: A mitochondrial visitor regulating damaged chromatin dynamics. *FEBS Lett* 592:172–178.
28. Sanderson TH, et al. (2013) Cytochrome *c* is tyrosine 97 phosphorylated by neuroprotective insulin treatment. *PLoS One* 8:e78627.
29. Hayashi T, et al. (2015) Higd1a is a positive regulator of cytochrome *c* oxidase. *Proc Natl Acad Sci USA* 112:1553–1558.
30. Pecina P, et al. (2010) Phosphomimetic substitution of cytochrome *C* tyrosine 48 decreases respiration and binding to cardiolipin and abolishes ability to trigger downstream caspase activation. *Biochemistry* 49:6705–6714.
31. García-Heredia JM, et al. (2011) Tyrosine phosphorylation turns alkaline transition into a biologically relevant process and makes human cytochrome *c* behave as an anti-apoptotic switch. *J Biol Inorg Chem* 16:1155–1168.
32. Kadenbach B, Urban PF (1968) Application of a quantitative chromatographic method of purification in the study of the biosynthesis of cytochrome *c*. *Fresenius Z Anal Chem* 243:542–554.
33. Guerra-Castellano A, et al. (2015) Mimicking tyrosine phosphorylation in human cytochrome *c* by the evolved tRNA synthetase technique. *Chemistry* 21:15004–15012.
34. Godoy LC, et al. (2009) Disruption of the M80-Fe ligation stimulates the translocation of cytochrome c to the cytoplasm and nucleus in nonapoptotic cells. *Proc Natl Acad Sci USA* 106:2653–2658.
35. Ying T, et al. (2009) Evolutionary alkaline transition in human cytochrome *c*. *J Bioenerg Biomembr* 41:251–257.
36. Schejter A, George P (1964) The 695-mμ band of ferricytochrome *c* and its relationship to protein conformation. *Biochemistry* 3:1045–1049.
37. Díaz-Moreno I, García-Heredia JM, Díaz-Quintana A, Teixeira M, De la Rosa MA (2011) Nitration of tyrosines 46 and 48 induces the specific degradation of cytochrome c upon change of the heme iron state to high-spin. *Biochim Biophys Acta* 1807:1616–1623.
38. Zaidi S, Hassan MI, Islam A, Ahmad F (2014) The role of key residues in structure, function, and stability of cytochrome-*c*. *Cell Mol Life Sci* 71:229–255.
39. Chothia C, Levitt M, Richardson D (1981) Helix to helix packing in proteins. *J Mol Biol* 145:215–250.
40. Pielak GJ, et al. (1995) Protein thermal denaturation, side-chain models, and evolution: Amino acid substitutions at a conserved helix-helix interface. *Biochemistry* 34: 3268–3276.
41. Ptitsyn OB (1998) Protein folding and protein evolution: Common folding nucleus in different subfamilies of *c*-type cytochromes? *J Mol Biol* 278:655–666.
42. Moreno-Beltrán B, et al. (2015) Respiratory complexes III and IV can each bind two molecules of cytochrome *c* at low ionic strength. *FEBS Lett* 589:476–483.
43. An H-J, et al. (2011) The survival effect of mitochondrial Higd-1a is associated with suppression of cytochrome C release and prevention of caspase activation. *Biochim Biophys Acta* 1813:2088–2098.
44. Chen YC, et al. (2012) Identification of a protein mediating respiratory supercomplex stability. *Cell Metab* 15:348–360.
45. Starkov AA, Fiskum G (2003) Regulation of brain mitochondrial H_2O_2 production by membrane potential and NAD(P)H redox state. *J Neurochem* 86:1101–1107.
46. de Vries S, Grivell LA (1988) Purification and characterization of a rotenone-insensitive NADH:Q6 oxidoreductase from mitochondria of *Saccharomyces cerevisiae*. *Eur J Biochem* 176:377–384.
47. Herrero E, Ros J, Bellí G, Cabiscol E (2008) Redox control and oxidative stress in yeast cells. *Biochim Biophys Acta* 1780:1217–1235.
48. Quinlan CL, et al. (2012) Mitochondrial complex II can generate reactive oxygen species at high rates in both the forward and reverse reactions. *J Biol Chem* 287: 27255–27264.
49. Dröse S (2013) Differential effects of complex II on mitochondrial ROS production and their relation to cardioprotective pre- and postconditioning. *Biochim Biophys Acta* 1827:578–587.
50. Grivennikova VG, Kozlovsky VS, Vinogradov AD (2017) Respiratory complex II: ROS production and the kinetics of ubiquinone reduction. *Biochim Biophys Acta* 1858: 109–117.
51. Guo J, Lemire BD (2003) The ubiquinone-binding site of the *Saccharomyces cerevisiae* succinate-ubiquinone oxidoreductase is a source of superoxide. *J Biol Chem* 278: 47629–47635.
52. Moreno-Beltrán B, et al. (2014) Cytochrome c1 exhibits two binding sites for cytochrome c in plants. *Biochim Biophys Acta* 1837:1717–1729.
53. Iverson SL, Orrenius S (2004) The cardiolipin-cytochrome *c* interaction and the mitochondrial regulation of apoptosis. *Arch Biochem Biophys* 423:37–46.
54. Namura S, et al. (1998) Activation and cleavage of caspase-3 in apoptosis induced by experimental cerebral ischemia. *J Neurosci* 18:3659–3668.
55. Cao G, et al. (2004) Cloning of a novel Apaf-1-interacting protein: A potent suppressor of apoptosis and ischemic neuronal cell death. *J Neurosci* 24:6189–6201.
56. García-Heredia JM, et al. (2010) Nitration of tyrosine 74 prevents human cytochrome c to play a key role in apoptosis signaling by blocking caspase-9 activation. *Biochim Biophys Acta* 1797:981–993.
57. García-Heredia JM, et al. (2012) Specific nitration of tyrosines 46 and 48 makes cytochrome *c* assemble a non-functional apoptosome. *FEBS Lett* 586:154–158.